Importance of Direct Metal−π Coupling in Electronic Transport Through Conjugated Single-Molecule Junctions

Jeffrey S. Meisner,[†,⊥] Seokhoon Ahn,[†,⊥] Sriharsha V. Aradhya,[‡] Markrete Krikorian,[†,∥] Radha Parameswaran,[§] Michael Steigerwald,*[†] Latha Venkataraman,*[‡] and Colin Nuckolls*[†]

[†]Department of Chemistry, Columbia University, New York, New York 10027, United States
[‡]Department of Applied Physics and Applied Mathematics, Columbia University, New York, New York 10027, United States
[§]Departments of Chemistry and Physics, Barnard College, New York, New York 10027, United States

Ⓢ *Supporting Information*

ABSTRACT: We study the effects of molecular structure on the electronic transport and mechanical stability of single-molecule junctions formed with Au point contacts. Two types of linear conjugated molecular wires are compared: those functionalized with methylsulfide or amine aurophilic groups at (1) both or (2) only one of its phenyl termini. Using scanning tunneling and atomic force microscope break-junction techniques, the conductance of mono- and difunctionalized molecular wires and its dependence on junction elongation and rupture forces were studied. Charge transport through monofunctionalized wires is observed when the molecular bridge is coupled through a S−Au donor−acceptor bond on one end and a relatively weak Au−π interaction on the other end. For monofunctionalized molecular wires, junctions can be mechanically stabilized by installing a second aurophilic group at the *meta* position that, however, does not in itself contribute to a new conduction pathway. These results reveal the important interplay between electronic coupling through metal−π interactions and quantum mechanical effects introduced by chemical substitution on the conjugated system. This study affords a strategy to deterministically tune the electrical and mechanical properties through molecular wires.
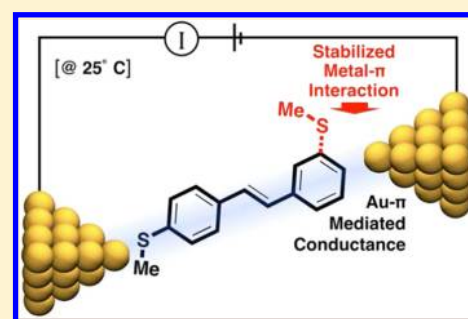
■ INTRODUCTION

This study describes the mechanism of conduction through asymmetric molecular junctions containing conjugated molecules having only one electrode-binding "linker" group.[1] Linker groups are aurophilic functional groups that bind the molecule between Au electrodes, such as thiols (−SH), primary amines (−NH$_2$), and methylsulfides (−SMe).[2] Typical molecules employed in single-molecule electronics are conjugated or short aliphatic molecules that are functionalized at each end with linker groups. Here, conjugated olefins of varying lengths are end-functionalized with methylsulfide and amine linkers at one or both terminal phenyl rings. To explore quantum mechanical effects[3] we vary the position of these linkers between the *meta* or *para* positions. The conductance and rupture forces of single-molecule junctions formed from these molecules are measured using the break-junction (BJ) technique with a scanning tunneling microscope (STM)[2a] and an atomic force microscope (AFM).[4] We find that for measurable conductivity to occur at least one of the rings must have a linker *para* to the olefin providing strong electronic coupling to the electrode. We measure both the highest conductivity and the narrowest distribution of conductance for olefins with two *para* linkers. When one of these *para* linkers is replaced with a *meta* linker, the conductance decreases by almost an order of magnitude, due to a reduction in the Au−molecule−Au coupling. If this mechanical contact, the *meta*

linker, is removed leaving only a single *para* linker, the conductance decreases even further. We show that the conductance of our molecular wires that have at least one *para* linker decays exponentially with increasing oligomeric length and that they have step lengths corresponding to their molecular length. Both of these results indicate that we are probing the conductance of single-molecule junctions, as opposed to junctions formed by overlapping or interdigitated molecular dyads. That is, these measurements allow us to conclude that monofunctionalized stilbene molecules do not readily form junctions where molecules conduct via intermolecular carrier transfer (i.e., π−π-stacking interactions).[5]

■ EXPERIMENTAL METHODS

Syntheses. For this study, we synthesized three different vinylogous series of methylsulfide-functionalized *trans*-α,ω-diphenyl-oligoenes as well as 3-(methylthio)stilbene. Each series ranges in length from the stilbene ($n = 1$) to the triene ($n = 3$) and is displayed in Figure 1A and 1B. A convenient shorthand is used to name these compounds (**PPn**, **PMn**, **Pn**, and **M1**), which includes the linker substitution (P = *para*, M = *meta*) and the length of the oligomer (n). As examples, **PP2** denotes *para−para′*-dithiomethyl-diphenylbutadiene and **PM3** denotes *para−meta′*-dithiomethyl-diphenylhexatriene. Both difunctionalized (**PPn** and **PMn**) and monofunctionalized (**Pn**
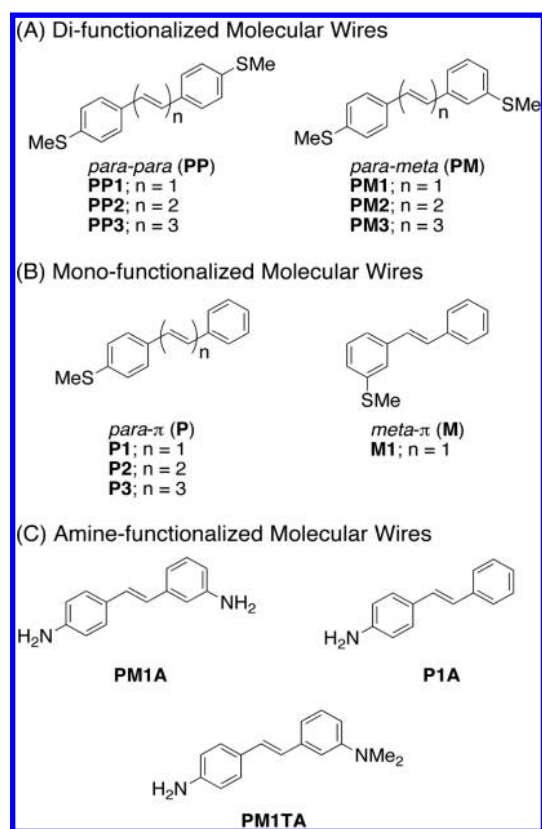
Figure 1. Chemical structures of *trans*-stilbene and all-*trans*-oligoene molecular wires: (A) difunctionalized series, having only *para*-positioned linker groups (**PPn**) or a mixture of *para* and *meta* linkers (**PMn**); (B) monofunctionalized wires **Pn** and **M1** contain either one *meta* or one *para* linker. (C) Stilbene derivatives end-functionalized with primary and tertiary amines.

and **M1**) molecules were synthesized through Wittig[6] and Horner−Wadsworth−Emmons reactions (see the Supporting Information for synthetic details and characterization).[7]

A set of three additional stilbene derivatives bearing amine linkers were synthesized to deconvolute the electronic and mechanical contributions in molecular junctions: (*E*)-3,4′-diaminostilbene (**PM1A**) and (*E*)-4-amino-stilbene (**P1A**) as analogous compounds to the conducting (*E*)-(methylthio)stilbenes above, as well as (*E*)-3-dimethylamino-4′-aminostilbene (**PM1TA**), where A = amine and TA = tertiary amine.

STM and AFM-BJ Measurements. STM-BJ measurements[2a,b] were performed in dilute solutions (1 ± 0.1 mM in 1,2,4-trichlorobenzene) of molecular wires using a gold-on-mica substrate and a gold STM tip (cut Au wire, 0.25 mm diameter, 99.998%, Alfa Aesar). Gold atomic point contacts were repeatedly formed and broken in the solution of molecules under a 500 mV voltage applied to the junction with a 100 kΩ resistor in series. As the point contacts are broken, one or a few molecules may bind to bridge the gap between the broken Au contact, thereby forming molecular junctions. The electrodes are then pulled farther apart until the junction is broken. Conductance (current/voltage) is measured as a function of piezo displacement yielding individual conductance traces. In doing so, our STM-BJ method does not take consecutive measurements on a single junction. Instead, at the end of each measurement the junction is destroyed. Then, before forming a new junction, the tip and substrate are smashed together and pulled apart, forming fresh electrodes and thus a new junction. For each molecule, over 5000 traces are collected and analyzed by creating one-dimensional (1D) conductance and two-dimensional (2D) conductance-displacement histograms[2d,8] that reveal statistically relevant information on junction conductance, as well its evolution under junction elongation.

Molecular conductance step lengths[9] and the slopes of the conductance features (β_S) in the 2D histograms were determined by fitting the average conductance profile; both procedures are outlined in detail in the Supporting Information.

Simultaneous conductance and force measurements were obtained using a custom-built conducting AFM setup.[4a] Single-molecule junctions were formed between a gold-coated commercial AFM cantilever (NanoAndMore, Inc.) and a gold-on-mica substrate. Conductance is measured across the tip/sample junction at a bias of 75 mV. The force is measured simultaneously by monitoring the deflection of a laser focused on the back of the cantilever. AFM-BJ measurements are carried out on **PP1**, **PM1**, and **P1**. In each case, 2D force-displacement histograms are constructed from measurements on over 8000 junctions.

Theoretical Methods. Density functional theory (DFT) electronic structure calculations examined shape and energy differences among the most relevant molecular orbitals (MOs) for molecular conductance. All calculations were preformed using Jaguar[10] with the B3LYP hybrid functional and the 6-31G** basis sets. The molecular geometries were fully optimized. The final geometries, total energies, and MO energies for each molecule in this study are given in the Supporting Information.

■ RESULTS AND DISCUSSION

We begin by comparing the conductance and rupture forces of molecular junctions of four stilbene derivatives having either one or two methylsulfide linkers in either the *meta* or *para* positions (**PP1**, **PM1**, **P1**, and **M1**). Their 1D logarithmically binned conductance histograms are obtained from STM-BJ measurements and are compared in Figure 2A. The histogram for **PP1** shows a clear molecular conductance peak, indicating that reproducible single-molecule junctions are formed throughout thousands of measurements. The sharpest peak at 10^{-3} G_0 is characteristic of a conjugated stilbene having two *para* linkers, as has been shown before.[3d,11] A characteristic conductance signature (peak in the histogram) appears for **P1** even though it contains only one linker. The peak conductance for **P1** is almost 2 orders of magnitude lower than that for **PP1**; therefore, electronic coupling across the **P1** junction is weaker than with **PP1**. From the width of the peak, we conclude that the junction conductance varies significantly more than in the case of **PP1**, which has two linkers. We quantify the peak width for all junctions in Table 1 using the half-width at half-maximum. We next compare **P1** with **M1**, which also has only one linker, but now at the *meta*-position, we see no peak in this histogram indicating that junctions with a conductance above our instrument noise ($\sim 10^{-7}$ G_0) are not formed with **M1**. This trend is expected since *meta* linkers do not provide strong electronic coupling into the π-system.[3a] Nonetheless, they do provide a mechanical link as we have previously shown.[3d] Indeed, we see with **PM1** that the additional mechanical stability provided by the *meta* linker yields both a higher conductance and a narrower distribution compared with **P1**. Conductance values for each compound are given in Table 1.

We confirm the mechanical enhancement provided by the *meta* linker by measuring force in AFM-BJs of **PP1**, **PM1**, and **P1**. The rupture forces are measured by pulling the junction apart until it breaks and (to a first-order approximation) establish an upper limit on the strength of the weakest Au−molecule interaction. Stilbenes with two methylsulfide linkers (regardless of their position on the phenyl rings) are stabilized in the junction and give rupture forces of 0.5 nN, as is the case with **PP1**[3d] and **PM1** (Figure 2C). In contrast, we found that the rupture force for **P1** is smaller than 0.3 nN (twice the instrumental noise). Our rupture force results for each stilbene
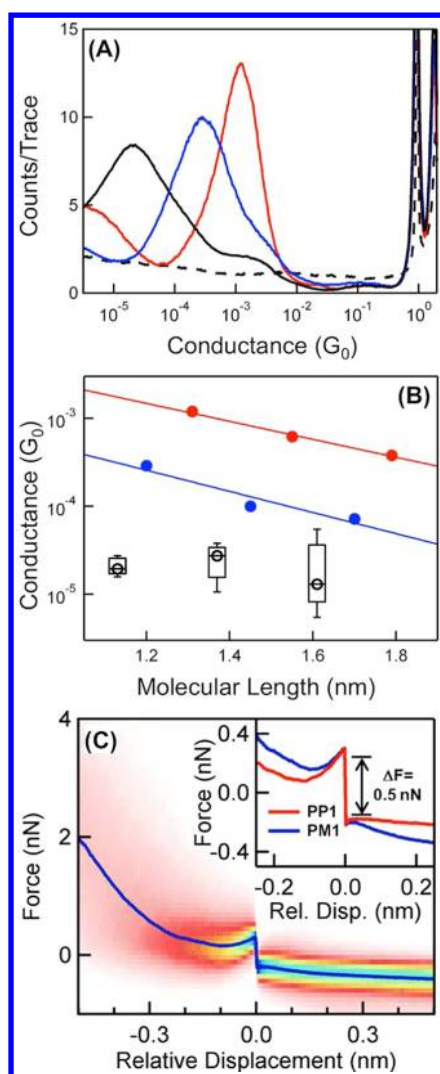
Figure 2. (A) 1D conductance histograms constructed using logarithmic bins for junctions of **PP1** (red), **PM1** (blue), **P1** (black), and **M1** (dashed). **M1** does not form conductive junctions. Histograms were generated from over 5000 traces without data selection, using 100 bins/decade. (B) Plot of molecular length vs conductance for *para–para* series (**PPn**; red) and *para–meta* series (**PMn**; blue). Exponential decay constants were found to be $\beta = 0.23 \pm 0.03$ and 0.27 ± 0.08 Å^{-1}, respectively. The effective contact resistance for **PPn** is 520 kΩ and for **PMn** is 1820 kΩ. Conductance for **Pn** (black) is represented with the mean peak conductance (black circles) within a distribution of the inner 50th percentile (black boxes) and the inner 80th percentile (bars). Due to junction-to-junction variations, larger samples sizes were used for **Pn** (over 30 000 individual conductance traces). (C) The 2D force histogram of **PM1** junctions compiled from ~8000 traces. The statistically averaged force profile (overlaid blue trace) shows an abrupt drop at zero-displacement of 0.5 nN corresponding to the average force required to rupture the junction. (Inset) Average force profiles from measurements of **PP1** and **PM1** junctions, which yield a rupture force of 0.5 nN for both.

Table 1. Tabulation of Conductance Parameters from STM-BJ Measurements

Molecule	1D Conductance Peak (G_0)	Conductance Peak Width[e]	Slope β_s (Å^{-1})	Step Length (nm)	Molecule Length[a] (nm)
PP1	1.2×10^{-3}	0.42	0.18	0.57	1.31[c]
PP2	6.2×10^{-4}	0.44	0.12	0.73	1.55[c]
PP3	3.8×10^{-4}	0.44	0.12	0.82	1.79[c]
PM1	2.9×10^{-4}	0.63	0.58	0.56	1.20[c]
PM2	1.0×10^{-4}	0.69	0.35	0.70	1.45[c]
PM3	7.2×10^{-5}	0.74	0.35	0.87	1.70[c]
P1	2.1×10^{-5}	0.90	0.67	0.61	1.13[d]
P2	2.6×10^{-5}	0.94	0.54	0.75	1.37[d]
P3	1.7×10^{-5}	1.02	0.46	0.86	1.61[d]
M1	n/a[b]	n/a[b]	n/a[b]	n/a[b]	1.00[d]
PM1A	2.2×10^{-4}	0.83	0.67	0.63	1.14[c]
P1A	2.8×10^{-5}	0.98	0.70	0.67	1.09[d]
PM1TA	2.8×10^{-5}	1.03	0.89	0.66	1.09[d]

[a]Molecular length is taken from DFT optimized structures. [b]Molecules do not form conductive junctions. [c]Length refers to the through-space distance between terminal linker group heteroatoms. [d]Length refers to the through-space distance from the *para*-linker group heteroatom to the most distant carbon atom. [e]Conductance peak widths are determined using the half-width at half-maximum on the high-conductance side of the peak, since low-conductance half-maxima are sometimes lost in the experimental noise.

result of a strengthened Au–π interaction, where the tunneling pathway is coupling directly into the π-space of the second ring while the *meta* linker secures that end to the electrode surface. Similar metal–π (Pt or Ag) interactions have been used to rationalize the conductance mechanism through symmetric metal–benzene–metal junctions at low temperature,[12] as well as molecular junctions of C_{60} and stacked oligomers of paracyclophane using Au electrodes at room temperature.[13]

To understand the conduction mechanism in greater detail, it is necessary to verify that conduction occurs through the molecular backbone of a single molecule. Therefore, we measured the length dependence of conductance through a series of oligomers **PPn**, **PMn**, and **Pn**, with $n = 1, 2,$ and 3. The peak conductance of each oligomer is given in Table 1. In Figure 2B, we plot the conductance histogram peaks against the molecular length for each series. The *para–para* bound series, **PPn**, is especially useful as a control group representing typical linear α,ω-diphenyl-oligoenes.[14] The decay constant (β), which describes the exponential decrease of conductance with increasing molecular length is found to be $\beta = 0.23 \pm 0.02$ Å^{-1}, in good agreement with published results.[15] For the **PMn** series, we also find an exponentially decreasing conductance with a decay constant of $\beta = 0.27 \pm 0.08$ Å^{-1}, which is similar to that of **PPn**. This indicates that conduction is through the π-system of a single molecule and not by any other mechanism, such as π–π-stacking between dimers.[5] When measuring conductance of the **Pn** series, we found that conductance peak values shifted within half of an order of magnitude over the course of the experiment (thousands of consecutive traces). The experimentally observed variation in conductance is illustrated by the error bars in Figure 2B (see the Supporting Information for details of the variability analysis). The

are overlaid in Figure 2C (inset). Consequently, the interaction between the Au electrode and unsubstituted phenyl ring does not contribute much to the mechanical stability of the junction at room temperature. Since linkers in the *meta* position behave as typical mechanical contacts (albeit without providing electrical coupling), we postulate that the conductance modulation found between the **PMn** and **Pn** series is the

variability increased with molecular length (**P1** < **P2** < **P3**), making it impossible to determine a valid decay constant.[16] Outside of the monosubstituted **Pn** series, the variation during and between different experimental runs (changing tip and substrate) caused insignificant variations in the most frequently measured conductance. This is typically the result obtained with methylsulfide linkers.

To further understand junction evolution, we show how the conductance changes during elongation. By constructing 2D conductance-displacement histograms, we can determine the maximal junction length, or step length, as well as trends in the molecule−electrode coupling. Figure 3A displays the 2D histograms[17] of the stilbenes junctions, **PP1**, **PM1**, and **P1** (all others are given in the Supporting Information). Their molecular conductance features extend about 0.6 nm. We note that they are ~0.7 nm shorter than the molecular lengths, which is common in STM-BJs due to snapback relaxations at the Au electrodes.[18] We quantify the step length for each
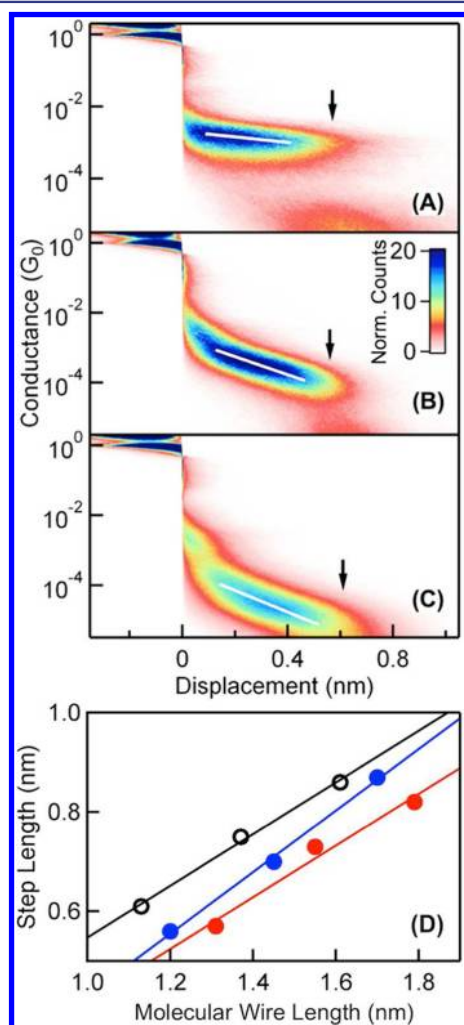
molecule as detailed in the Supporting Information and summarize them in Table 1. For each oligomeric series, the step length increases linearly with molecular backbone length (Figure 3D).[2c] The fact that all three molecular systems scale linearly with molecular wire length, and with similar slopes, indicates that in each case the molecular junctions are formed with only a single molecule. The step lengths of **Pn** are slightly longer (0.02−0.04 nm) than those of **PPn**. We attribute the difference to changes in the linker group[2c] (*para*-SMe vs Au−π) and not the formation of π−π-stacked dimers since significantly larger step lengths would then be expected.

The 2D histograms also show that the slope of the conductance-versus-displacement curves changes significantly between each series in the order, **PPn** > **PMn** > **Pn**. The white lines overlaid in Figure 3A−C represent the statistically averaged decreasing conductance, whose slopes are tabulated in Table 1 for all our molecules. Steeper slopes correspond to junctions whose conductance decreases with elongation due to weaker metal−molecule coupling. For **PMn** and **Pn** series, where conduction occurs through π−metal overlap, the conductance should depend sensitively on junction geometry, and specifically, conductance should decrease as the area of overlap between the electrode and the molecular backbone is decreased with increasing elongation.

Since the conductance of the **PPn** series is systematically higher than the corresponding **PMn** series, and since *meta*-substitution appears to be nonconductive, our data suggest that conduction in **PMn** junctions occurs through the combination of a Au−S interaction in the *para*-substituted ring and a direct Au−π interaction in the *meta*-substituted ring. To verify this hypothesis, and to distinguish the role of the linker at the meta position from its electronic influence into the π-system, we employed a series of amine-terminated stilbenes where, in contrast to the methylsulfide stilbenes, we are able to retain electronic effects while disrupting the mechanical coupling at the *meta*-linker (**PM1A** and **PM1TA** from Figure 1C). Molecules terminated with primary amines (RNH_2) bind to the Au electrodes, forming molecular junctions in the STM-BJ setup. However, when primary amines are methylated to form tertiary amines ($RNMe_2$), they do not bind to Au.[2b] In this way, the linker group's electron-donating contributions to the MOs are preserved while arresting additional mechanical stabilization.

Conductance histograms of **PM1A**, **P1A**, and **PM1TA** junctions are compared in Figure 4. The conductance peak for the *para*−*meta* bound junction (**PM1A**) is almost an order of magnitude higher than that of the *para*−π bound junction (**P1A**), similar to what was observed for the methylsulfide analogues (**PM1** vs **P1**). However, when the *meta*-NH$_2$ of **PM1A** is replaced by *meta*-NMe$_2$, the conductance of the resulting **PM1TA** drops by an order of magnitude, overlapping the conductance of monofunctionalized **P1A**. With these direct structural comparisons, we conclude that the electrical pathway in the *para*−*meta* bound series is through a Au−π interaction and that the *meta* linker serves as a mechanical stabilizer that enhances the electronic coupling between the terminal phenyl group and the Au electrode.

Theoretical Analysis. To gain insight into the electronic structure of our molecular junctions, DFT calculations were carried out to examine the shape of MOs. The methylsulfide-functionalized stilbenes (**PP1**, **PM1**, and **P1**) are considered. The most relevant MOs are those nearest to the Fermi level of the electrodes. Since these junctions are generally highest-
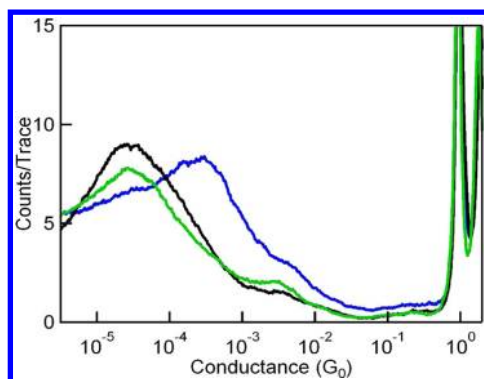

Figure 3. 2D conductance-displacement histograms are generated from over 5000 individual measurements on (A) **PP1**, (B) **PM1**, and (C) **P1** single-molecule junctions. Colored contour represents the number of counts × 1000. Step lengths are marked by black arrows, representing the 90th percentile of conductance, at 0.57, 0.56, and 0.61 nm, respectively. (D) Plot of the step lengths vs molecular wire lengths of **PPn** (red), **PMn** (blue), and **Pn** (black) series, with slopes of 0.52, 0.62, and 0.52, respectively. Molecular wire lengths were determined by DFT calculations.

Figure 4. Log-binned conductance histograms of amine-functionalized stilbene molecular wires: *para−meta* **PM1A** (blue), *para−π* **P1A** (green), and methylated *para−meta* **PM1TA** (black) were generated from 5000 individual conductance traces.

occupied molecular orbital (HOMO) conducting,[19] we examine the HOMO, HOMO-1, and HOMO-2 of **PP1** and **PM1**, which contain the p−π orbitals of sulfur and the olefin (C=C), as well as the HOMO and HOMO-1 for compounds **P1**. Since other MOs are much lower in energy, their contributions become negligible.

First, we inspect the results of the *para−para* case (**PP1**), which are shown in Figure 5A. We see that the orbitals are strongly coupled across the molecular backbone and include both sulfur lone pairs (S_{LP}). In contrast, the two S_{LP}'s in the *para−meta* compound (**PM1**; Figure 5B) are decoupled. In fact, the energy cost to mix these orbitals and establish a conduction pathway (through each S_{LP}) is roughly equal to the energetic cost (∼0.85 eV) required to disrupt that in the previous case (**PP1**). In light of this, it would be reasonable to expect **PM1** to not conduct at all. However, upon deeper inspection we find density located on the phenyl ring opposite the *para* linker and purpose this as an alternative conduction pathway. This secondary path is also predicted to exist in **PP1**; however, since it is expected to be more resistive, it may not be experimentally distinguishable in **PP1**. In the special case of **PM1**, the secondary path may be the only available conductance pathway.

For the *para−π* bound molecule (**P1**; Figure 5) the ring systems and S_{LP} are strongly coupled to one another. Due to the lack of a second linker, a single conductance pathway exists in **P1**, which closely resembles that of the secondary path found in **PM1**, leading to conducting junctions, despite lacking in the mechanical stability provided by a second linker. This MO interpretation helps to identify relationships linking the intrinsic properties of the bridging molecule with the conductance mechanism and overall device performance. Further studies that include the mapping of the density of states and couplings of the Au electrodes are beyond the scope of this study. Our theoretical results agree with our experimental findings and give weight to a dominant secondary pathway in **PM1** that is similar to that found in **P1**.

◼ CONCLUSION

The mechanism of conductance through monofunctionalized single-molecule wires was determined by measuring the electrical and mechanical properties in single-molecule junctions. By using a combination of rational molecular design, STM- and AFM-BJ techniques, we showed that mono- and difunctionalized molecular wires conduct through the backbone
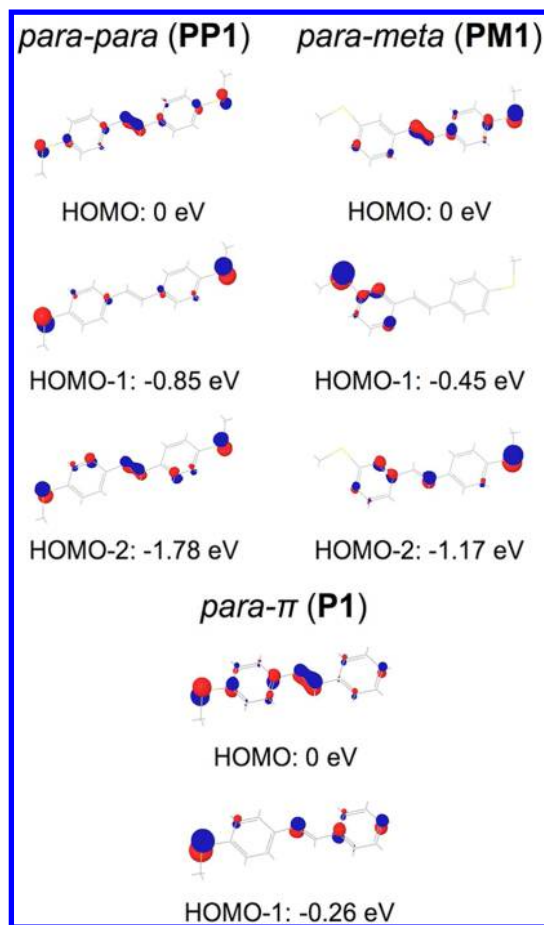

Figure 5. DFT calculated isosurfaces of MOs relevant in single-molecule conductance. Geometries of **PP1**, **PM1**, and **P1** were optimized and MOs calculated at the B3LYP/6-31** level of theory in the gas phase. HOMO energies were normalized to 0 eV for easy comparison. Contour values set at 0.75.

of a single molecule rather than though π−π-stacked dimers. The conductance mechanism differs between the *para−para* bound (**PPn**) and *para−π* bound molecules (**Pn**, **P1A**, and **P1TA**). Since the **Pn** series is functionalized with only one linker, a mechanically weak, yet electronically coupled, Au−π interaction completes the molecular circuit. The limited strength of this new interaction causes significant variability in junction-to-junction conductance. However, installing a second linker at the *meta* position stabilizes this interaction by securing the terminal phenyl group to the electrode surface, such as for the *para−meta* compounds (**PMn** and **PM1A**). *Meta* linkers result in quantum electronic interference effects that suppress the conductance, but the position of the linkers (*meta* vs *para*) does not significantly alter their mechanical attachment to the Au electrodes. By exploiting this attribute we strengthen a direct molecule−metal interaction that dominates in the charge transport of monofunctionalized molecular junctions, in turn enabling us to quantify the charge transport properties arising from Au−π interactions. This strategy may prove useful in future molecular-scale device architectures for the positioning of molecules onto electrode surfaces while mediating their electronic couplings, such as is needed for advancement in single-molecule rectification.[20]

■ ASSOCIATED CONTENT

ⓢ Supporting Information

Synthetic details and characterization data for all compounds; details of experimental setup and analysis methods; theoretical methods and tabulated results. This material is available free of charge via the Internet at http://pubs.acs.org.

■ AUTHOR INFORMATION

Corresponding Author
mls2064@columbia.edu; lv2117@columbia.edu; cn37@columbia.edu

Present Address
∥Department of Chemistry, Massachusetts Institute of Technology, Cambridge, MA.

Author Contributions
⊥These authors contributed equally.

Notes
The authors declare no competing financial interest.

■ ACKNOWLEDGMENTS

■ REFERENCES

(1) (a) Diez-Perez, I.; Hihath, J.; Lee, Y.; Yu, L.; Adamska, L.; Kozhushner, M. A.; Oleynik, I. I.; Tao, N. *Nature Chem.* **2009**, *1*, 635. (b) Kim, B.; Choi, S. H.; Zhu, X. Y.; Frisbie, C. D. *J. Am. Chem. Soc.* **2011**, *133*, 19864. (c) Holmlin, R. E.; Haag, R.; Chabinyc, M. L.; Ismagilov, R. F.; Cohen, A. E.; Terfort, A.; Rampi, M. A.; Whitesides, G. M. *J. Am. Chem. Soc.* **2001**, *123*, 5075.

(2) (a) Xu, B. Q.; Tao, N. J. *Science* **2003**, *301*, 1221. (b) Venkataraman, L.; Klare, J. E.; Tam, I. W.; Nuckolls, C.; Hybertsen, M. S.; Steigerwald, M. L. *Nano Lett.* **2006**, *6*, 458. (c) Park, Y. S.; Whalley, A. C.; Kamenetska, M.; Steigerwald, M. L.; Hybertsen, M. S.; Nuckolls, C.; Venkataraman, L. *J. Am. Chem. Soc.* **2007**, *129*, 15768. (d) Martin, C. A.; Ding, D.; Sorensen, J. K.; Bjornholm, T.; van Ruitenbeek, J. M.; van der Zantt, H. S. J. *J. Am. Chem. Soc.* **2008**, *130*, 13198. (e) Hong, W.; Manrique, D. Z.; Moreno-García, P.; Gulcur, M.; Mishchenko, A.; Lambert, C. J.; Bryce, M. R.; Wandlowski, T. *J. Am. Chem. Soc.* **2011**, *134*, 2292.

(3) (a) Mayor, M.; Weber, H. B.; Reichert, J.; Elbing, M.; von Hanisch, C.; Beckmann, D.; Fischer, M. *Angew. Chem., Int. Ed.* **2003**, *42*, 5834. (b) Solomon, G. C.; Andrews, D. Q.; Hansen, T.; Goldsmith, R. H.; Wasielewski, M. R.; Van Duyne, R. P.; Ratner, M. A. *J. Chem. Phys.* **2008**, 129. (c) Ke, S. H.; Yang, W. T.; Baranger, H. U. *Nano Lett.* **2008**, *8*, 3257. (d) Aradhya, S. V.; Meisner, J. S.; Krikorian, M.; Ahn, S.; Parameswaran, R.; Steigerwald, M. L.; Nuckolls, C.; Venkataraman, L. *Nano Lett.* **2012**, *12*, 1643. (e) Guedon, C. M.; Valkenier, H.; Markussen, T.; Thygesen, K. S.; Hummelen, J. C.; van der Molen, S. J. *Nat. Nanotechnol.* **2012**, *7*, 305.

(4) (a) Frei, M.; Aradhya, S. V.; Koentopp, M.; Hybertsen, M. S.; Venkataraman, L. *Nano Lett.* **2011**, *11*, 1518. (b) Xu, B. Q.; Xiao, X. Y.; Tao, N. J. *J. Am. Chem. Soc.* **2003**, *125*, 16164.

(5) π−π-staking in STM-BJs has been previously reported; however, many experimental factors were different from our study, including the structure of their bridging molecules, longer molecular lengths, and different solvent system during their STM-BJ measurements. See: Wu, S. M.; Gonzalez, M. T.; Huber, R.; Grunder, S.; Mayor, M.; Schonenberger, C.; Calame, M. *Nat. Nanotechnol.* **2008**, *3*, 569.

(6) Wittig, G.; Schollkopf, U. *Chem. Ber.* **1954**, *87*, 1318.

(7) Wadsworth, W. S. In *Org. React.*; John Wiley & Sons, Inc.: New York, 1977; Vol. 25, p 73.

(8) Kamenetska, M.; Koentopp, M.; Whalley, A.; Park, Y. S.; Steigerwald, M.; Nuckolls, C.; Hybertsen, M.; Venkataraman, L. *Phys. Rev. Lett.* **2009**, *102*, 126803.

(9) Parameswaran, R.; Widawsky, J. R.; Vazquez, H.; Park, Y. S.; Boardman, B. M.; Nuckolls, C.; Steigerwald, M. L.; Hybertsen, M. S.; Venkataraman, L. *J. Phys. Chem. Lett.* **2010**, *1*, 2114.

(10) *Jaguar*, 7.8 ed.; Schrodinger, L.L.C.: New York, NY, 2011.

(11) Widawsky, J. R.; Kamenetska, M.; Klare, J.; Nuckolls, C.; Steigerwald, M. L.; Hybertsen, M. S.; Venkataraman, L. *Nanotechnology* **2009**, *20*, 434009.

(12) (a) Kiguchi, M.; Tal, O.; Wohlthat, S.; Pauly, F.; Krieger, M.; Djukic, D.; Cuevas, J. C.; van Ruitenbeek, J. M. *Phys. Rev. Lett.* **2008**, *101*, 046801. (b) Kiguchi, M.; Miura, S.; Takahashi, T.; Hara, K.; Sawamura, M.; Murakoshi, K. *J. Phys. Chem. C* **2008**, *112*, 13349.

(13) (a) Schneebeli, S.; Kamenetska, M.; Cheng, Z.; Skouta, R.; Friesner, R. A.; Venkataraman, L.; Breslow, R. *J. Am. Chem. Soc.* **2011**, *133*, 2136. (b) Park, H.; Park, J.; Lim, A.; Anderson, E.; Alivisatos, A.; McEuen, P. *Nature* **2000**, *407*, 57. (c) Schull, G.; Frederiksen, T.; Arnau, A.; Sanchez-Portal, D.; Berndt, R. *Nature Nanotechnol.* **2011**, *6*, 23. (d) Neel, N.; Kroeger, J.; Limot, L.; Palotas, K.; Hofer, W. A.; Berndt, R. *Phys. Rev. Lett.* **2007**, *98*, 016801.

(14) **PPn**, **PMn**, and **Pn** represent the first oligoene series having no main-chain functionalizations to be studied in STM-BJs or other single-molecule methods. Other oligoene systems studied are based on carotenoid or α,ω-diphenyl-μ,ν-dicyano structures, which are decorated with methyl or cyano groups along the conjugated backbone (see: ref 15).

(15) (a) Meisner, J. S.; Kamenetska, M.; Krikorian, M.; Steigerwald, M. L.; Venkataraman, L.; Nuckolls, C. *Nano Lett.* **2011**, *11*, 1575. (b) He, J.; Chen, F.; Li, J.; Sankey, O. F.; Terazono, Y.; Herrero, C.; Gust, D.; Moore, T. A.; Moore, A. L.; Lindsay, S. M. *J. Am. Chem. Soc.* **2005**, *127*, 1384.

(16) Large variability in the junction conductance of the **Pn** series results in a range in the estimation of the decay constant ($0 > \beta > 0.46$ Å^{-1}).

(17) 2D histograms are generated using an automated algorithm with the added requirement that a G_0 break is clearly identifiable in the trace (more than 80% of the traces that start with a conductance greater than 1 G_0 and successfully break satisfy this requirement). In 2D histograms the conductance is binned logarithmically with 200 bins per decade in conductance (*y*-axis), while displacement is binned linearly (*x*-axis).

(18) Immediately after the formation of gold point contact electrodes, surface adatoms quickly reorganize, thus widening the distance between the electrodes. We refer to this as the "snapback" distance. This was first discovered during measurements at 4 K: (a) Yanson, A. I.; Bollinger, G. R.; van den Brom, H. E.; Agrait, N.; van Ruitenbeek, J. M. *Nature* **1998**, *395*, 783. For room temperature: (b) Quek, S. Y.; Kamenetska, M.; Steigerwald, M. L.; Choi, H. J.; Louie, S. G.; Hybertsen, M. S.; Neaton, J. B.; Venkataraman, L. *Nat. Nanotechnol.* **2009**, *4*, 230.

(19) (a) Venkataraman, L.; Park, Y. S.; Whalley, A. C.; Nuckolls, C.; Hybertsen, M. S.; Steigerwald, M. L. *Nano Lett.* **2007**, *7*, 502. (b) Ma, G. H.; Sun, L. L.; Zhang, R. X.; Shen, Z. Y.; Hou, S. M. *Chem. Phys.* **2010**, *375*, 67. (c) Li, Z.; Kosov, D. S. *Phys. Rev. B* **2007**, *76*, 035415. (d) Quek, S. Y.; Venkataraman, L.; Choi, H. J.; Louie, S. G.; Hybertsen, M. S.; Neaton, J. B. *Nano Lett.* **2007**, *7*, 3477.

(20) Aviram, A.; Ratner, M. A. *Chem. Phys. Lett.* **1974**, *29*, 277.